Effect of Shell-Side Flows on Hollow-Fiber Membrane Device Performance

Joe Lemanski and G. Glenn Lipscomb
Dept. of Chemical Engineering, University of Cincinnati, Cincinnati, OH 45221

Membrane-based separation processes are the preferred choice to accomplish many industrial separations. Among the numerous applications are filtration, dialysis, reverse osmosis, and gas separations (Ho and Sirkar, 1992).

Modules utilizing hollow-fiber membranes are efficient contactors. As shown in Figure 1, a typical module contains a hollow-fiber bundle potted at each end to form tubesheets that are encased in and sealed to an external shell. This arrangement allows for the introduction and removal of fluids separately from the fiber interior (lumen-side) and exterior (shell-side) spaces. The resulting device is the mass-transfer equivalent of a shell-and-tube heat exchanger.

For design purposes, analyses of how these devices perform require knowledge of the membrane mass-transfer properties and the nature of the flow in both the lumen and shell. Such analyses typically assume that all fibers possess the same size and mass-transfer characteristics. Additionally, most analyses assume that the shell and lumen flows are cocurrent, countercurrent, or cross-current to one another (Hwang and Kammermeyer, 1975; Mulder, 1991).

Detailed analyses of the fluid mechanics within membrane modules are available in the literature. However, to the best of our knowledge, no work exists that addresses fluid distribution across the fiber bundle. The heat-transfer literature does partially address the distribution of fluid across the tubes in a shell-and-tube heat exchanger (Palen and Taborek, 1962; Pekdemir et al., 1993; Baptista and Castro, 1993; Thomas, 1993). However, much of this work is either based on empirical correlations or not readily applicable to hollow fiber bundles due to differences in the size and number of tubes.

We present a theoretical analysis of shell-side flows and their influence on mass transfer. The general problem is computationally quite complex. We consider only the simplest, nontrivial effects here, but within a framework that is readily modified to allow examination of other issues associated with shell-side flows.

Model Development

Paths that fluid elements take through the shell (the streamlines) are illustrated in Figure 2; details of the calculations used to obtain Figure 2 are given in the Results section. The amount of time a fluid element contacts the membrane depends on the streamline it follows. This residence time distribution arises from the need to distribute fluid *across* the fiber bundle before it can flow *along* the fiber bundle.

The difference in shell fluid paths affects module performance in three ways. First, the extent of mass transfer varies from streamline to streamline due to the residence time distribution; the greatest concentration changes occur in fluid elements with the longest residence times. Second, different fluid elements move parallel to (co- or countercurrent flow) and perpendicular to (cross-flow) the fibers for different periods of time; this impacts the driving force for mass transfer. Third, the fluid mass-transfer resistance is a function of the local velocity field; concentration boundary layers grow more quickly, so mass-transfer coefficients are smaller for flows

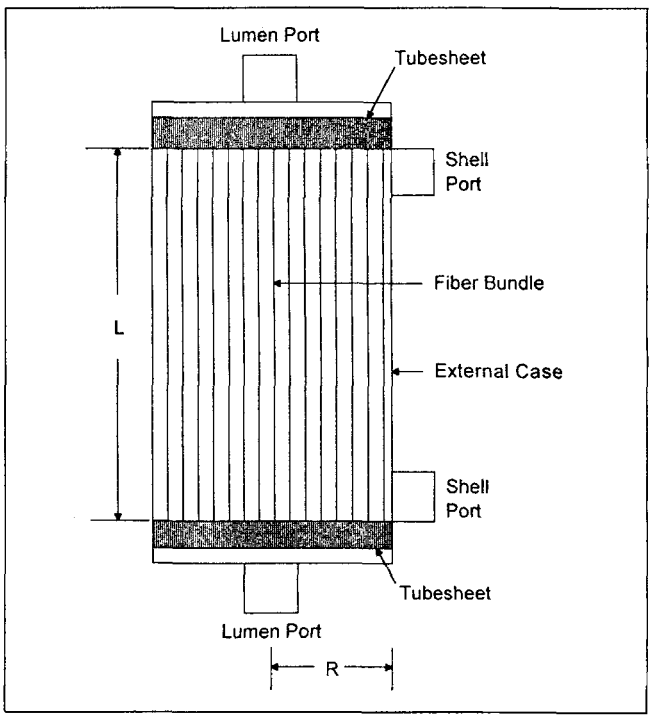

Figure 1. Typical hollow-fiber module.

Correspondence concerning this article should be addressed to G. G. Lipscomb who is currently at the Dept. of Chemical Engineering, University of Toledo, Toledo, OH 43606.

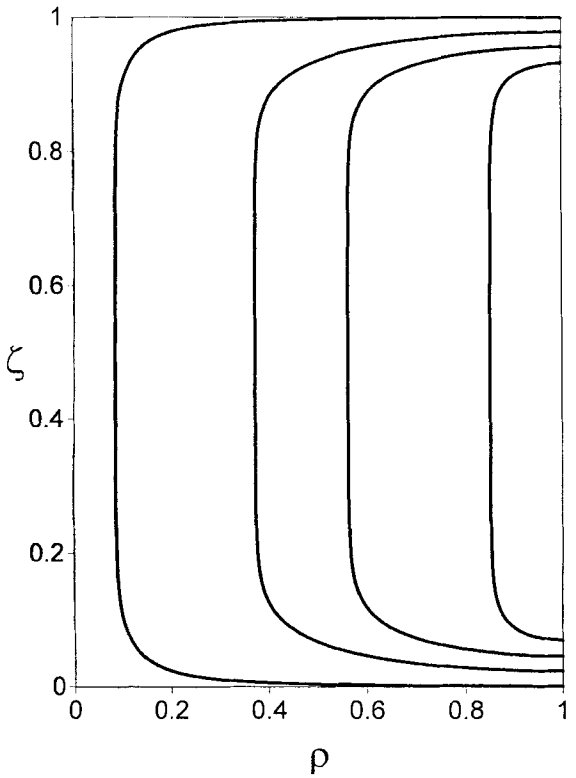

Figure 2. Paths that fluid elements may take through the shell of a hollow fiber bundle.

Streamlines calculated for $MG = 55$. See text for details of calculations.

parallel (co- or countercurrent) to the fiber bundle than perpendicular (cross-flow) (Wickramasinghe et al., 1992; Costello et al., 1993).

Addressing each of these issues comprehensively is a task of great complexity. In this work, we isolate and examine the first issue only. How does the shell residence time distribution affect hollow fiber membrane device performance? With this goal in mind, we assume the lumen side fluid concentration remains constant and the membrane poses the greatest resistance to mass transfer, which allows us to avoid the issue of concentration boundary layer growth and co- vs. cross- vs. countercurrent flow.

A numerical approximation for the velocity field at all points in-between fibers in the shell requires discretization of a large, complex domain. To simplify this task, one can volume average (Bear and Verruijt, 1987; Kaviany, 1991) the governing conservation equations over length scales small compared to the overall shell dimensions but large relative to the spacing in-between fibers. The volume-averaged equations describe transport in an effective homogeneous medium instead of the actual heterogeneous shell region.

Volume averaging (Kaviany, 1991; Quintard and Whitaker, 1993) yields Darcy's law as the relationship between volume average velocity ($\bar{u}$) and gradient of volume average pressure (p) (Whitaker, 1986; Barrère et al., 1992),

$$\bar{u} = -\frac{1}{\mu}(\bar{\bar{\kappa}}\cdot\nabla p) \tag{1}$$

where $\bar{\bar{\kappa}}$ is the Darcy permeability tensor and μ is the fluid viscosity; note that hydrostatic pressure differences are neglected. Equation 1 is rigorously valid only for low Reynolds number flows of Newtonian fluids where $Re = (\bar{u}/\epsilon)l/\nu$, $\bar{u}/\epsilon$ is a characteristic fluid velocity within the void space of the porous medium, l is a characteristic length scale of the pore structure (such as interfiber spacing), and ν is the fluid kinematic viscosity.

For isotropic porous media, the Darcy permeability tensor, $\bar{\bar{\kappa}}$, reduces to a scalar permeability constant. However, in axisymmetric, aligned fiber bundles, one would expect the relationship between velocity and pressure gradient to be different for flows *along* and *across* the fiber bundle. For such cases, the Darcy permeability tensor is given by,

$$\bar{\bar{\kappa}} = \begin{bmatrix} \kappa_{rr} & 0 \\ 0 & \kappa_{zz} \end{bmatrix}, \tag{2}$$

where values of κ_{rr} and κ_{zz} are given in Table 1 for a range of porosities and fiber packings.

Considering the removal of dilute solutes only from the shell-side fluid, volume averaging the steady-state overall conservation of mass equation yields

$$0 = \nabla\cdot\bar{u} = \frac{\kappa_{rr}}{\gamma}\frac{\partial}{\partial\gamma}\left(\gamma\frac{\partial p}{\partial r}\right) + \kappa_{zz}\frac{\partial^2 p}{\partial z^2}, \tag{3}$$

where the second equality follows from Eqs. 1 and 2.

Neglecting mass transfer by shell-side diffusion or Taylor dispersion relative to convection, volume averaging the conservation of mass equation for the dilute solute yields (Carbonell and Whitaker, 1983),

$$\bar{u}\cdot\nabla c_s = -(ka)c_s = \frac{Dc_s}{Dt}, \tag{4}$$

where c_s is the shell volume average solute concentration, k is the intrinsic mass-transfer coefficient, a is the area for mass transfer per unit shell volume, and D/Dt denotes the substantial derivative. In writing Eq. 4, we assume the lumen concentration is zero and ϵ varies over length scales much larger than the length scales over which the velocity and concentration vary.

Table 1. Values of κ_{rr} and κ_{zz} as a Function of Fiber Packing Geometry and Fiber Packing Fraction ($f = 1 - \epsilon$)

Packing Geometry	Packing Fraction	$\kappa_{rr}(m^2 \times 1E10)$	$\kappa_{zz}(m^2 \times 1E10)$	κ_{rr}/κ_{zz}
Square array	0.4	7.1	19	0.37
	0.5	2.3	8.4	0.27
	0.6	0.58	3.8	0.15
Triangular array	0.4	7.2	17	0.42

Source: Happel and Brenner, 1965; Skartsis et al., 1992.

To neglect diffusive mass transfer relative to convection, the Peclet number, defined as $Pe_m = \bar{u}L/D_m$, must be large, where L is a characteristic dimension of the fiber bundle (such as radius or length) and D_m is the molecular diffusivity of the solute. Likewise, to neglect Taylor dispersion effects, the Peclet number evaluated using the Taylor diffusivity must be large. Since D_T is proportional to $(\bar{u}l)^2/D_m$ (Koch et al., 1989), this is equivalent to requiring $Pe_T \propto (L/l)^2/Pe_m$ to be large. One cannot increase both Pe_m and Pe_T without increasing the separation of the macro- and microscopic length scales, that is, the magnitude of the ratio L/l. For example, to ensure both Peclet numbers are greater than 100, L/l must be greater than $10(Pe_m)^{0.5}$ (more specifically, if $Pe_m = 100$, L/l must be greater than 100 to neglect Taylor dispersion).

Integration of Eq. 4 along streamlines gives the concentration of different fluid elements at the shell outlet. Integrating this expression for concentration with respect to the fluid residence time distribution (RTD) gives the change in mixing cup average concentration between the shell inlet and outlet,

$$(\Phi)_M = \frac{(c_s)_M}{(c_s)_i} = \int_0^\infty e^{-kat} E(t)\,dt = \int_0^\infty (ka) e^{-kat} F(t)\,dt, \quad (5)$$

where $E(t)dt$ is the fraction of the fluid that spends some time between t and $t + dt$ in contact with the membrane and $F(t)$ is the fraction of fluid that spends some time t or less in contact with the membrane (Levenspiel, 1972).

For design purposes, a useful performance measure is the ratio of the mass-transfer coefficient required to predict performance, assuming all fluid elements contact the membrane for one space time, $\tau = \epsilon V/Q$ (that is, plug flow at the volume average velocity) to the actual, intrinsic mass-transfer coefficient. This ratio is given by

$$\frac{\bar{k}}{k} = -\frac{\ln\left((ka)\int_0^\infty e^{-kat} F(t)\,dt\right)}{ka\tau}, \quad (6)$$

where $\bar{k}$ is the required *effective* mass-transfer coefficient and V is the total device volume, $\pi R^2 L$.

To determine the fluid residence time distributions, one must first solve Eq. 3 for the pressure field. Integrating along the streamlines of the velocity field obtained from Eqs. 1 and 2 gives the residence time distribution that enters Eq. 6 for the effective mass-transfer coefficient.

One can nondimensionalize Eqs. 1–6 by defining the following dimensionless variables: $\rho = r/R$, $\zeta = z/L$, $\theta = t/\tau$, and $P = (p - p_i)/(p_o - p_i)$. Upon doing so, two dimensionless groups appear: the module geometry number, $MG = (\kappa_{rr}/\kappa_{zz})(L/R)^2$, and the mass-transfer number $MT = ka\tau$. Specifying values for these two groups completely determines the solution for the effective mass-transfer coefficient.

Solution Methodology

The results presented here are limited to the specific module geometry illustrated in Figure 3. We assume the fiber bundle is axisymmetric and consists of fibers aligned parallel to each other in the axial direction. The dimensions indicated in Figure 3 correspond to the dimensions of an Althin hemodialyzer (Althin, 1992).

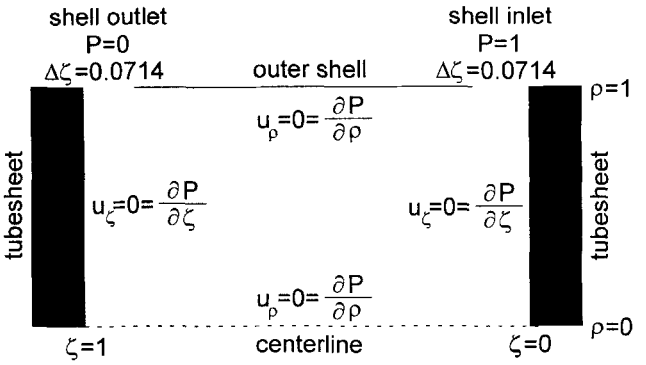

Figure 3. Module geometry and boundary conditions used in the numerical calculations.

Appropriate boundary conditions for Eq. 3 are also indicated in Figure 3. Along the shell inlet and outlet P is assumed to be a constant, equal to 1 and 0, respectively. This boundary condition assumes that the fluid is uniformly distributed around the outside of the fiber bundle at both the inlet and outlet without significant pressure loss. A large, open annular region exists around the fiber bundle near each port to help ensure uniform fluid distribution in the Althin device. One cannot state unequivocally that fluid distribution is uniform for all modules, but we do not know of any theoretical analysis of this effect. Furthermore, a detailed study of this three-dimensional flow problem would warrant a separate investigation. Along all other boundaries the velocity component normal to the boundary is assumed to be equal to zero. Note that the tangential velocity may be nonzero for flows governed by Darcy's law.

The potential equation for P, Eq. 3, is solved using a finite difference numerical approximation. Central difference approximations are used for all first- and second-order derivatives, except along domain boundaries where first-order derivatives are represented with appropriate second-order differences (Anderson et al., 1984). The residence time distribution was evaluated from the velocity field using Euler's method. Finally, a mesh-refinement study was conducted to ensure that the numerical approximation error did not affect the results.

Results

The streamlines computed for $MG = 55$ are shown in Figure 2. Note that different fluid elements traverse different distances from inlet to outlet. Fluid elements entering near the tubesheet travel the greatest distance, while fluid elements entering near the shell travel the shortest distance.

Figure 4 shows the corresponding residence time distributions computed for a range of MG values. Decreasing MG increases the breadth of the F curve while the fraction of fluid that spends one space time in the shell or less, $F(\theta = 1)$, decreases.

Figure 5 shows the variation of $\bar{k}/k$ with MT for various values of MG. The values of $\bar{k}/k$ vary from approximately 0.7 to 1.1 for all cases. For small MT, the effective mass-transfer coefficient increases as MG decreases. Values greater than unity are even predicted for the lowest values of MG. As MT increases, $\bar{k}/k$ decreases for all values of MG. The rate of decrease is more rapid for small MG, so the

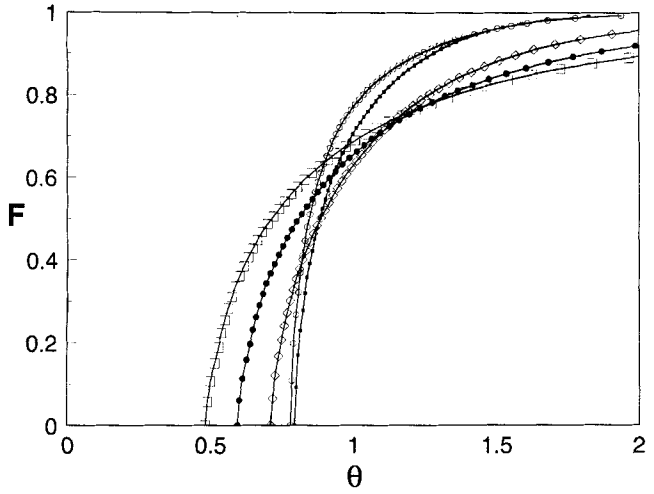

Figure 4. Computed residence time distributions for various values of *MG*.

Open square, 1; filled circle, 2; open diamond, 5; filled square, 75; open circle, 150.

value of *MG* corresponding to the maximum effective mass-transfer coefficient shifts to an intermediate value.

Discussion

We can use the RTD to rationalize the preceding results. The discussion is based on three features of the RTD: (1) $F(\theta = 1)$, (2) the width of the small θ tail, and (3) the width of the large θ tail. To quantify the latter two features, we use the value of θ for which F first becomes nonzero (the shortest contact time, θ_{min}) and equals 0.98 (an estimate of the longest contact time, θ_{max}), respectively (Table 2).

Fluid elements that contact the membrane for a time greater than one space time will experience greater mass transfer than *average*; *average* refers to the performance of fluid elements that spend one space time in contact with the membrane consistent with the definition of $\bar{k}/k$. The converse applies to fluid elements that spend less than one space time in contact with the membrane.

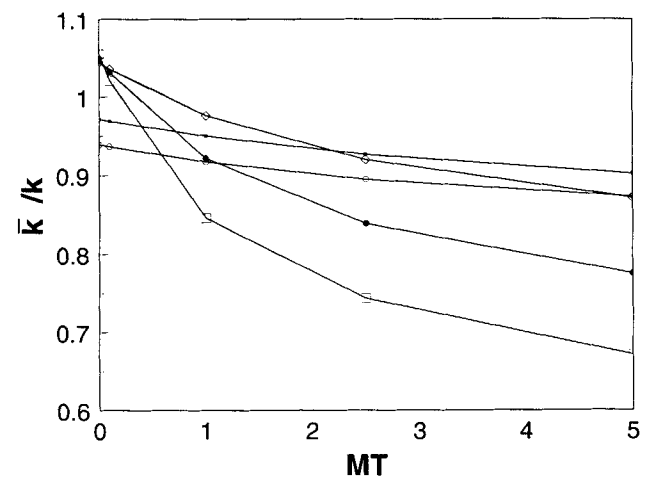

Figure 5. Dependence of $\bar{k}/k$ on *MT* for various values of *MG*.

Open square, 1; filled circle, 2; open diamond, 5; filled square, 75; open circle, 150.

Table 2. Values of $F(1)$, θ_{max} and θ_{min} as a Function of MG

MG	$F(1)$	$\theta_{max} = \theta(0.98)$	θ_{min}
1	0.69	4.1	0.48
2	0.66	3.1	0.59
5	0.63	2.4	0.71
75	0.71	1.7	0.79
150	0.77	1.7	0.78

For small *MT* (that is, high flow rates for fixed membrane properties), the overall mass transfer is low. The mass transfer that occurs in fluid elements that contact the membrane for one space time or less is *very* low and does not vary significantly. Thus, the short residence time tail has little impact on performance, and performance is dominated by the long residence time tail. The largest tails, as indicated by the values of $F(1)$ and θ_{max}, occur for the smallest values of *MG* and give the largest values of $\bar{k}/k$. The performance enhancement due to the long residence time tail may be so significant that the effective mass-transfer coefficient exceeds the intrinsic mass-transfer coefficient.

As *MT* increases (flow rate decreases), the effective mass-transfer coefficient decreases as fluid elements that contact the membrane for less than one space time become detrimental to performance. The smallest tails, as indicated by the values of $F(1)$ and θ_{min}, occur for the largest values of *MG* giving the smallest declines in the effective mass-transfer coefficient. The effective mass-transfer coefficient is virtually constant for large *MG*, but dramatic decreases occur for small *MG*.

Values of *MG* for many commercial hollow fiber membrane modules appear to fall in the range 10–100; Table 3 shows specific commercial designs. Typical commercial devices possess an aspect ratio of 5–10 and a fiber packing fraction of roughly 0.4–0.6. For these parameter ranges, *MG* varies from approximately 6 to 60. Our calculations suggest that in this range, module performance is high but not too sensitive to fluid flow rate or *MT*. Thus, it represents a desirable design.

For what separations are the results most applicable? The primary assumptions of constant membrane-dominated mass-transfer resistance, removal of dilute solutes, and constant lumen concentration dictate the answer. Such separations would include (1) removal of dilute species from gases with highly selective membranes [such as water (Wang et al., 1992)], (2) gas absorption with chemical reaction (Qi and Cussler, 1985; Yang and Cussler, 1986), (3) perstraction with a receiving fluid that has a high capacity for the solute (Sirkar, 1992), and (4) dialysis of high molecular weight species with high dialysate flow rates (Kessler and Klein, 1992).

How significant are the performance differences in comparison to other uncertainties in the design equations and experimental limitations? One would not expect a 10% change in the mass-transfer coefficient to be experimentally verifiable. However, the 40% change predicted for values of *MG* less than ~ 1 would be. Moreover, such performance drops are often attributed to fiber packing nonuniformities [fluid bypass (Noda et al., 1979; Seibert et al., 1993)], but this work shows that even uniformly packed bundles can possess "bypasslike" effects and a lower design limit exists for *MG*.

Table 3. Approximate Values of *MG* for Commercial Hollow-Fiber Membrane Devices

Manufacturer	*MG*
Althin Altra Flux Hemodialyzer (Althin, 1992)	50–75
Hoechst Celanese Liqui-Cel (Sirkar, 1992; Seibert et al., 1993)	100–400
Sepracor Hollow Fiber Dialyzers (Kessler and Klein, 1992)	50–100
Enka Cupraphan Hollow Fiber Dialyzers (Kessler and Klein, 1992)	10–20
Bend Research Dehydration Module (Wang et al., 1993)	> 1,000

Conclusions

Fluid flow within the shell of a hollow fiber bundle is analyzed based on volume averaging of the relevant conservation of mass and momentum equations. The ratio of the effective mass-transfer coefficient to the intrinsic mass-transfer coefficient of the fiber depends on two dimensionless groups: module geometry number, *MG*, and intrinsic mass-transfer coefficient number, *MT*. For small *MT*, the best performance is found for small values of *MG*. However, upon increasing *MT*, performance decreases dramatically for small *MG*, while little change occurs for large *MG*. Therefore, the best overall performance is found for large *MG*.

The performance changes are interpreted in terms of the residence time distribution. For small *MT*, the large θ behavior of *F* controls performance, while the small θ behavior controls performance for large *MT*. Commercial module designs appear to favor *MG* values of order magnitude 10 for which the *MT* dependence of performance is small.

Acknowledgment

The authors acknowledge partial support of this work by the National Science Foundation through grant CTS-9408414.

Notation

E = differential residence time distribution
f = fiber packing fraction
F = cumulative residence time distribution
n = unit normal
Q = volumetric flow rate (m^3/s)
r = radial coordinate (m)
R = fiber bundle radius (m)
u = velocity (m/s)
z = axial coordinate (m)
ϵ = fiber bundle void fraction
ζ = dimensinoless axial coordinate
θ = dimensionless residence time
ρ = density (kg/m^3) or dimensionless radial coordinate
Φ = dimensionless concentration change

Subscripts and superscripts

i = inlet
M = mixing cup average
o = outlet
r = radial

Literature Cited

Althin CD Medical, Inc., Product Information Literature (1992).
Anderson, D. A., J. C. Tannehill, and R. H. Pletcher, *Computational Fluid Mechanics and Heat Transfer*, Hemisphere, New York (1984).
Baptista, C. G., and J. A. Castro, "Cell Models for the Shell-Side Flow in Multitubular Reactors," *Ind. Eng. Chem. Res.*, **32**, 1093 (1993).
Barrère, J., O. Gipouloux, and S. Whitaker, "On the Closure Problem for Darcy's Law," *Trans. Porous Media*, **7**, 209 (1992).
Bear, J., and A. Verruijt, *Modeling Groundwater Flow and Pollution*, Reidel, Dordrecht, The Netherlands (1987).
Carbonell, R. G., and S. Whitaker, "Dispersion in Pulsed Systems: II. Theoretical Developments for Passive Dispersion in Porous Media," *Chem. Eng. Sci.*, **38**, 1795 (1983).
Costello, M. J., A. G. Fane, P. A. Hogan, and R. W. Schofield, "The Effect of Shell Side Hydrodynamics on the Performance of Axial Flow Hollow Fibre Modules," *J. Memb. Sci.*, **80**, 1 (1993).
Happel, J., and H. B. Brenner, *Low Reynolds Number Hydrodynamics*, Prentice-Hall, Englewood Cliffs, NJ (1965).
Ho, W. S., and K. K. Sirkar, eds., *Membrane Handbook*, Van Nostrand Reinhold, New York (1992).
Hwang, S.-T., and K. Kammermeyer, *Membranes in Separations*, Wiley, New York (1975).
Kaviany, M., *Principles of Heat Transfer in Porous Media*, Springer-Verlag, New York (1991).
Kessler, S. B., and E. Klein, "Dialysis," *Membrane Handbook*, W. S. Ho and K. K. Sirkar, eds., Van Nostrand Reinhold, New York (1992).
Koch, D. L., R. G. Cox, H. Brenner, and J. F. Brady, "The Effect of Order on Dispersion in Porous Media," *J. Fluid Mech.*, **200**, 173 (1989).
Levenspiel, O., *Chemical Reaction Engineering*, Wiley, New York (1972).
Mulder, M., *Basic Principles of Membrane Technology*, Kluwer, Boston (1991).
Noda, I., D. G. Brown-West, and C. C. Gryte, "Effect of Flow Maldistribution on Hollow Fiber Dialysis—Experimental Studies," *J. Memb. Sci.*, **5**, 209 (1979).
Palen, J. W., and J. Taborek, "Solution of Shell Side Flow Pressure Drop and Heat Transfer by Stream Analysis Method," *AIChE Symp. Ser.*, **65**(92), 53 (1962).
Pekdemir, T., T. W. Davies, L. E. Haseler, and A. D. Diaper, "Flow Distribution on the Shellside of a Cylindrical Shell and Tube Heat Exchanger," *Int. J. Heat Fluid Flow*, **14**, 76 (1993).
Qi, Z., and E. L. Cussler, "Microporous Hollow Fibers for Gas Absorption: II. Mass Transfer across the Membrane," *J. Memb. Sci.*, **23**, 333 (1985).
Quintard, M., and S. Whitaker, "Transport in Ordered and Disordered Porous Media: Volume-averaged Equations, Closure Problems, and Comparison with Experiment," *Chem. Eng. Sci.*, **48**, 2537 (1993).
Seibert, A. F., X. Py, M. Mshewa, and J. R. Fair, "Hydraulics and Mass Transfer Efficiency of a Commercial-Scale Membrane Extractor," *Sep. Sci. Tech.*, **28**, 343 (1993).
Sirkar, K. K., "Other New Membrane Processes," *Membrane Handbook*, W. S. Ho and K. K. Sirkar, eds., Van Nostrand Reinhold, New York (1992).
Skartsis, L., B. Khomami, and J. L. Kardos, "Resin Flow Through Fiber Beds During Composite Manufacturing Processes: I. Review of Newtonian Flow Through Fiber Beds," *Poly. Eng. Sci.*, **32**, 221 (1992).
Thomas, L. C., *Heat Transfer*, Prentice-Hall, Englewood Cliffs, NJ (1993).
Wang, K. L., S. H. McCray, D. D. Newbold, and E. L. Cussler, "Hollow Fiber Air Drying," *J. Memb. Sci.*, **72**, 231 (1992).
Whitaker, S., "Flow in Porous Media I: A Theoretical Derivation of Darcy's Law," *Trans. Porous Media*, **1**, 3 (1986).
Wickramasinghe, S. R., M. J. Semmens, and E. L. Cussler, "Mass Transfer in Various Hollow Fiber Geometries," *J. Memb. Sci.*, **69**, 235 (1992).
Yang, M. C., and E. L. Cussler, "Designing Hollow Fiber Contactors," *AIChE J.*, **32**, 1910 (1986).

Manuscript received July 18, 1994, and revision received Nov. 17, 1994.